

# The Detection Rates of Merging Binary Black Holes Originating from Star Clusters and Their Mass Function

Michiko S. FUJII<sup>1</sup>, Ataru TANIKAWA,<sup>2</sup> and Junichiro MAKINO<sup>3,4</sup>

<sup>1</sup>Department of Astronomy, Graduate School of Science, The University of Tokyo,  
7-3-1 Hongo, Bunkyo-ku, Tokyo, 113-0033, Japan

<sup>2</sup>Department of Earth Science and Astronomy, College of Arts and Sciences, The University  
of Tokyo,

3-8-1 Komaba, Meguro-ku, Tokyo 153-8902, Japan

<sup>3</sup>Department of Planetology, Graduate School of Science, Kobe University,  
1-1, Rokkodai-cho, Nada-ku, Kobe, Hyogo, Japan, 657-8501

<sup>4</sup>RIKEN Advanced Institute for Computational Science,  
7-1-26 Minatojima-minami-machi, Chuo-ku, Kobe, Hyogo 650-0047, Japan

\*E-mail: fujii@astron.s.u-tokyo.ac.jp

Received ; Accepted

## Abstract

Advanced LIGO achieved the first detection of the gravitational wave, which was from a merging binary black hole (BBH). In the near future, more merger events will be observed, and the mass distribution of them will become available. The mass distribution of merger events reflects the evolutionary path of BBHs: dynamical formation in dense star clusters or common envelope evolution from primordial binaries. In this paper, we estimate the detection rate of merging BBHs which dynamically formed in dense star clusters by combining the results of  $N$ -body simulations, modeling of globular clusters, and cosmic star-cluster formation history. We estimate that the merger rate density in the local universe within the redshift of 0.1 is  $13\text{--}57 \text{ Gpc}^{-3} \text{ yr}^{-1}$ . We find that the detection rate is 0.23–4.6 per year for the current sensitivity limit and that it would increase to 5.1–99 per year for the designed sensitivity which will be achieved in 2019. The distribution of merger rate density in the local universe as a function of redshifted chirp mass has a peak close to the low-mass end. The chirp mass function of the detected mergers, on the other hand, has a peak at the high-mass end, but is almost flat. This difference is simply because the detection range is larger for more massive BBHs.

**Key words:** gravitational waves — globular clusters: general — galaxies: star clusters: general

## 1 Introduction

The detection of the gravitational wave (GW) source GW150914 by the Laser Interferometer Gravitational Wave Observatory (LIGO) was interpreted as the merger of a binary black hole (BH) whose members have masses of  $m_1 = 36^{+5}_{-4} M_\odot$  and  $m_2 = 29^{+4}_{-4} M_\odot$  (Abbott et al. 2016b). The gravitational wave has finally become the reality, and advanced

LIGO (aLIGO) opens up a new window to observe the universe.

What we have seen through this newly opened window is quite a big surprise in the sense that it was not a merger event of a binary neutron star (NS). Previous studies of the event rate before the detection of GW150914 generally concluded that the detection rate of NS-NS mergers is higher than that of BH-BH mergers by more than one order of magnitude (e.g., Abadie et al.

2010).

One obvious reason that researchers did not expect the merging of two  $30\text{-}M_{\odot}$  BHs as the dominant sources of GW events is simply that there was no observational evidence for BHs with a mass more than  $10M_{\odot}$ , except for those of supermassive BHs at the centers of galaxies and only a few evidences of intermediate-mass black holes (IMBHs) (Farrell et al. 2009).

On the other hand, once found, it looks rather natural that a BBH merger was detected rather than NS-NS mergers. The detected GW event (35–250 Hz) (Abbott et al. 2016b) is in the frequency range for which aLIGO has high sensitivity. The merging of two  $30\text{-}M_{\odot}$  BHs generates GW with 20 times larger amplitude, compared to that generated by the merging of two  $1.4\text{-}M_{\odot}$  NSs. Even if the sensitivity is the same, the limit distance for the detection of merging of two  $30\text{-}M_{\odot}$  BHs is 20 times larger than that for NS-NS mergers. When converted to the search volume, the difference is as large as  $10^4$ . Therefore, if the event rate of  $30\text{-}M_{\odot}$  BH mergers is larger than  $10^{-4}$  of the rate of NS-NS mergers, GW events observed by aLIGO and other ground-based detectors will be dominated by binaries with  $30\text{-}M_{\odot}$  or more massive BHs. In fact, the distance of GW150914 is 400 Mpc, while the current detection limit of aLIGO for NS-NS mergers is only around 80 Mpc (Abbott et al. 2016b, 2016c). There is nearly an order of magnitude difference between the actual distance of the observed GW event and the current limit for NS-NS merger events. Previous theoretical studies indeed predicted the detection rate of BBH mergers is roughly two orders of magnitude higher than that of NS-NS mergers (Bae et al. 2014; Dominik et al. 2015). In addition, recent stellar evolution models with updated stellar wind models suggest that massive BHs with a mass of up to  $80M_{\odot}$  easily form from single massive stars (Vink 2008). Some recent studies have predicted that massive BBH mergers would be detected more frequently than NS-NS mergers (Belczynski et al. 2010; Downing et al. 2011; Mapelli et al. 2013; Rodriguez et al. 2015).

What GW150914 tells us are (a) the gravitational wave from merging of BHs really exists and is observed, and (b) there are BHs with a mass more than  $10M_{\odot}$ , and some of them do form binaries which merge within the Hubble time. From the observational point of view, we can expect that a large number of event in this mass range will be observed, and the precise mass function and even the redshift distribution will be determined in the near future. From the theoretical point of view, key questions posed by GW150914 are how  $30\text{-}M_{\odot}$  BHs formed and how they ended up in binaries and eventually merged. A related important question is whether they fill the gap between observed stellar-mass BHs and supermassive BHs.

Traditional models for the formation channels of BBHs are (a) common envelope evolution of primordial binary massive stars (Belczynski et al. 2007) and (b) dynamical formation in dense star clusters (Portegies Zwart & McMillan 2000).

Recently, rather exotic formation models such as the fission of the degenerated core during the gravitational collapse has been proposed (Loeb 2016), but the validity of such models is yet to be confirmed.

For the dynamical formation scenario, Tanikawa (2013) performed a series of  $N$ -body simulations of star clusters and modeled BBH merger history based on the results of the simulations. They estimated the merger rate of BBHs originating from globular clusters which were born either 10 or 12 Gyr ago, assuming a number density of globular clusters in the universe (similar studies have also been done by O’Leary et al. 2006; Banerjee et al. 2010). In this paper, we present an improved estimate for the merger rate, detection rate, mass function, and the redshift dependence for BBH mergers, using the updated sensitivity of current and future LIGO (Kissel 2015; Abbott et al. 2016c), global star formation history (Madau & Dickinson 2014), and the initial mass function (IMF) of BHs.

Our main findings are summarized as follows. The dynamical formation of BBHs in star clusters prefers the formation of binaries of the most massive BHs with the mass ratio rather close to unity. Thus, the total event rate (not considering the sensitivity of the detector) peaks at the chirp mass of around  $10M_{\odot}$ , but the event rate for  $30\text{--}50\text{-}M_{\odot}$  events is around 1/10 of that for  $10M_{\odot}$ . When we take into account the detector sensitivity, the event rate becomes almost flat for the range of the chirp mass of 10 to  $100\text{-}M_{\odot}$ . The merger rate in the local universe ( $z < 0.1$ ) is estimated to be  $13\text{--}57\text{ Gpc}^{-3}\text{ yr}^{-1}$ , which is consistent with the value estimated from aLIGO ( $9\text{--}240\text{ Gpc}^{-3}\text{ yr}^{-1}$  The LIGO Scientific Collaboration et al. 2016). The detection rates are estimated to be 0.23–4.6 and 5.1–99 per year for the current and future sensitivity limits, respectively.

## 2 Methods

We estimate the merger rate of BBHs dynamically formed in star clusters, combining BBH merger histories modeled from the results of  $N$ -body simulations of star clusters (Tanikawa 2013) with a globular cluster formation history following a cosmic star formation rate. We follow the method of Tanikawa (2013) (see also O’Leary et al. 2006; Downing et al. 2011), but we adopt a time-depending number density of globular clusters ( $n_{\text{GC}}$ ) assuming that the number of forming star clusters is proportional to the cosmic star formation rate. We finally calculate the detection rate of BBH merger events by means of aLIGO assuming a power spectral density of aLIGO (Kissel 2015; Abbott et al. 2016c). In the following, we describe the details of our methods.

## 2.1 Model for BH merger history per globular cluster

Tanikawa (2013) performed a series of  $N$ -body simulations of isolated globular clusters and modeled the merger event history of the escaping BBHs. In globular clusters, the separation of binaries shrink due to three-body interactions, and if they become tight enough, they are ejected from the clusters. Once BBHs are ejected, they experience no more encounter. The orbital parameters when they escape determine their merger timescale due to GW radiation. From the escaping rates and the distribution of orbital parameters of escaping BBHs, we can estimate the merger rate of BBHs dynamically formed in globular clusters. We here summarize the  $N$ -body simulations and modeling in Tanikawa (2013) and then describe our modified model.

### 2.1.1 Summary of Tanikawa (2013)

In Tanikawa (2013), a series of direct  $N$ -body simulations of star clusters was performed for three different values of the initial densities of star clusters. The initial mass functions were given by Kroupa's mass function (Kroupa 2001) with a mass range of  $0.1\text{--}50M_\odot$ , and the initial distribution of stars followed a King model (King 1966) with a dimensionless concentration parameter  $W_0 = 7$ . Simulations were performed using NBODY4 (Aarseth 2003), in which stellar and binary evolution models (Hurley et al. 2000, 2001) were included. For massive stars, however, a model suggested by Eldridge & Tout (2004) was used. The metallicity was assumed to be  $Z = 0.001$ . The relation between the zero-age main-sequence (ZAMS) stellar mass and the resulting BH mass is shown in Figure 1 (same as Figure 1 in Tanikawa 2013). With these models, the maximum mass of BHs is  $\sim 20M_\odot$ . In Figure 2, we present the BH mass function resulting from these models.

The number of particles of the simulations were  $N = 8000\text{--}10^5$  because it is still difficult to perform a large- $N$  simulations up to  $N \sim 10^6$ . In Tanikawa (2013), instead, they confirmed that the cumulative number of BBH escaping from star clusters is written as a function of the thermodynamical time,  $\tau$ , which is given by

$$\tau = \int_0^t \frac{dt'}{t_{\text{rh}}}, \quad (1)$$

where  $t_{\text{rh}}$  is half-mass relaxation time given by

$$t_{\text{rh}} = 0.0477 \frac{N}{\sqrt{G\rho_h} \log(0.4N)} \quad (2)$$

(Spitzer 1987). Here,  $\rho_h$  and  $N$  are the half-mass density and the number of particles, respectively. Tanikawa (2013) found that the cumulative number of BBH escapers irrespective of BH mass is obtained from the  $N$ -body simulations as

$$N_{\text{BBH,esc}}(\tau) = 0.020 N_{\text{BH,i}} \tau, \quad (3)$$

where  $N_{\text{BH,i}}$  is the number of BHs obtained from the IMF. Using this function, we can estimate a merger rate per cluster

**Table 1.** Models of star clusters

Model	$N$	$m_{\text{BH,max}}(M_\odot)$	$M_{\text{cl}}(M_\odot)$	$N_{\text{BH,i}}$
Small ( $54M_\odot$ )	$5 \times 10^5$	54	$3.1 \times 10^5$	919
Small ( $20M_\odot$ )	$5 \times 10^5$	20	$3.1 \times 10^5$	715
Middle ( $54M_\odot$ )	$10^6$	54	$6.1 \times 10^5$	1839
Middle ( $20M_\odot$ )	$10^6$	20	$6.1 \times 10^5$	1430
Large ( $54M_\odot$ )	$2 \times 10^6$	54	$1.2 \times 10^6 M_\odot$	3677
Large ( $20M_\odot$ )	$2 \times 10^6$	20	$1.2 \times 10^6 M_\odot$	2860

For all models,  $W_0 = 7$  and  $\rho_h = 10^5 M_\odot \text{pc}^{-3}$  are used.

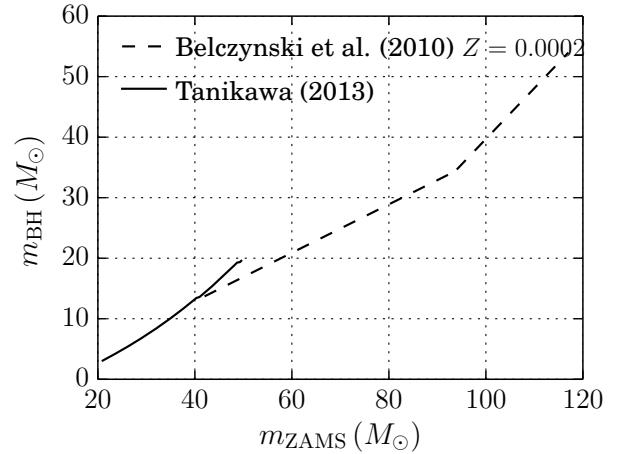


**Fig. 1.** Relation between ZAMS and BH masses adopted in Tanikawa (2013) (full line) and obtained by Belczynski et al. (2010) (dashed line).

with a given number of particles.

In Tanikawa (2013), three models with different numbers of particles ( $N = 5 \times 10^5$ ,  $10^6$ , and  $2 \times 10^6$ ) are adopted. They correspond to  $3.1 \times 10^5$ ,  $6.1 \times 10^5$ , and  $1.2 \times 10^6 M_\odot$ , respectively assuming the mean stellar mass is  $0.61M_\odot$ . We call these models small, middle, and large, respectively. We adopt an initial half-mass density of  $10^5 M_\odot \text{pc}^{-3}$ , which is typical for globular clusters (Heggie & Giersz 2008; Giersz & Heggie 2009, 2011) and the middle density model in Tanikawa (2013). We summarize the models of star clusters in Table 1.

From the results of the  $N$ -body simulations, Tanikawa (2013) also obtained the primary mass of BBHs ( $m_1$ ), mass ratio ( $q = m_2/m_1$ ), eccentricity, and semi-major axis distributions of escaping BBHs. They confirmed that these do not depend on  $N$ . They modeled these distributions by fitting a function to the results of their simulations. We hereafter describe their models.

The probability distribution as a function of BH mass ratio ( $q$ ), eccentricity ( $e$ ), and semi-major axis ( $a$ ) obtained from the simulations are expressed as

$$P_1(q) = \begin{cases} 0 & (\text{for } 0 < q < 0.5), \\ \int_{0.5}^q 2dq' & (\text{for } 0.5 < q < 1) \end{cases} \quad (4)$$

(see equations (12) and (13) in Tanikawa 2013),

$$P_2(e) = \int_0^e 2e' de' \quad (5)$$

(see equations (10) and (11) in Tanikawa 2013), and

$$P_3(a) = \int_0^a p_3(a') da', \quad (6)$$

where

$$p_3(a) = \frac{1}{\sqrt{2\pi}\sigma(a/a_{1kT})} \exp \left[ -\frac{1}{2\sigma^2} \left\{ \log \left( \frac{a}{a_{1kT}} \right) - \log \mu \right\}^2 \right] \quad (7)$$

(see equations (8) and (9) in Tanikawa 2013), respectively. Here,  $\sigma = 0.81$  and  $\mu = 0.15$  (Tanikawa 2013), and  $a_{1kT}$  is a semi-major axis with which the binding energy of a binary is  $1kT$ , where  $3/2kT$  is the initial average kinetic energy of stars in the star cluster. The relation between the primary mass of BBH mass ( $m_1$ ) and the escape time of the BBH in thermodynamical time of the cluster ( $\tau$ ) is given by

$$m_1(\tau) = \begin{cases} 20M_\odot & (0.5 < \tau < 1.5), \\ 20M_\odot \left( \frac{\tau}{1.5} \right)^{-1} & (\tau > 1.5) \end{cases} \quad (8)$$

(see equation (14) in Tanikawa 2013).

Using these functions, we can generate a distribution of escaping BBHs per cluster by means of a Monte Carlo technique and then calculate their merging timescale due to the GW radiation, which is given by

$$t_{\text{GW}} = \frac{5}{256} \frac{c^5}{G^3} \frac{a^4}{m_1^3 q(1+q)} g(e), \quad (9)$$

where

$$g(e) = \frac{(1-e^2)^{3.5}}{1 + (73/24)e^2 + (37/96)e^4}. \quad (10)$$

Here  $c$  is the light speed.

### 2.1.2 Generating BBH Merger History per Cluster

Using equations (1)–(10), we construct merger event histories for each cluster model. In the top left panel of Figure 2, we present the mass function of BHs which contribute to BBH mergers ( $m_1$  and  $m_2$ ) up to a cluster age of 12 Gyr for our three cluster models. From the stellar evolution models that we adopt, the lower-mass limit of BHs is set to be  $3M_\odot$ . For comparison, we also show the BH mass distribution obtained from the adopted IMF and stellar evolution model. We confirmed that the numbers of BHs which contribute to BBH mergers generated from our model do not exceed the number of BBHs expected from the IMF. We also present the chirp mass function in the top right panel of Figure 2. The merger rates per cluster per 1 Gyr are presented in Figure 3. For all models, the merger rates decrease with time. Although Tanikawa (2013) varied the initial density of globular clusters, we adopt that for their standard model ( $10^5 M_\odot \text{pc}^{-3}$ ).

In Tanikawa (2013), the maximum mass of BHs was limited to  $20M_\odot$  because their IMF was limited to  $50M_\odot$  (see Figure 1). On the other hand, the BH masses observed by GW were  $\sim 30M_\odot$  (Abbott et al. 2016b), and as a consequence, we cannot estimate the merger rates of such massive BBHs with their model. We therefore modify the model given by Tanikawa (2013) to include more massive BHs. Equation (8) gives the

relation between the primary mass of BBH mass ( $m_1$ ) and the escape time of the BBH ( $\tau$ ). This relation shows that in star clusters with a realistic mass function, massive stars sink to the cluster core quickly and tend to form hard binaries due to the mass segregation. As a result, more massive binaries escape earlier from the star cluster. Since  $N$ -body simulations performed by Tanikawa (2013) had an upper limit of the BH mass of  $20M_\odot$ , all escapers in  $\tau < 1.5$  is assumed to have the maximum BH mass. We change this assumption to that the escape time of the BBH ( $\tau$ ) continuously decreases up to a new maximum BH mass because if star clusters contain more massive BHs, it is natural to consider that they have shorter escape time. We therefore extrapolate equation (8) to a new upper-mass limit ( $54M_\odot$ ), which is the maximum BH mass which can avoid the pair instability supernova range (Belczynski et al. 2014). This new relation is expressed as

$$m_1(\tau) = \begin{cases} 54M_\odot & (0.5 < \tau < 0.55), \\ 20M_\odot \left( \frac{\tau}{1.5} \right)^{-1} & (\tau > 0.55). \end{cases} \quad (11)$$

The distributions of the generated merging BH mass and the chirp mass are presented in the bottom panels of Figure 2. We assume that the probability distributions for  $q$ ,  $e$ , and  $a$  do not change. The obtained merger rates are shown in Figure 3. At 0–1 Gyr, the merger rates are slightly higher than those for the models with a maximum BH mass of  $20M_\odot$ . This is because more massive BHs have a shorter merger time.

In order to compare these results with models that directly constructed from the results of  $N$ -body simulations, we also present the BH mass function obtained from IMF up to  $120M_\odot$  in the bottom left panel of Figure 2. Here, we assume a stellar evolution model which gives a relation between ZAMS and BH masses shown in Figure 1 (Belczynski et al. 2010). Here,  $Z = 0.0002$  is assumed. For  $m_{\text{ZAMS}} < 42M_\odot$ , the result is consistent with that of Tanikawa (2013). For simplicity, we adopted

$$m_{\text{BH}}(M_\odot) = \begin{cases} 0.52(M_{\text{ZAMS}}/1M_\odot) - 8.1 & (21 < M_{\text{ZAMS}}/1M_\odot < 42) \\ 0.40(M_{\text{ZAMS}}/1M_\odot) - 3.1 & (42 < M_{\text{ZAMS}}/1M_\odot < 94) \\ 0.84(M_{\text{ZAMS}}/1M_\odot) - 44 & (94 < M_{\text{ZAMS}}/1M_\odot < 120) \end{cases}$$

which is obtained by a least-squares fitting to the models of Belczynski et al. (2010) and Tanikawa (2013). The small discrepancy around  $40$ – $50M_\odot$  in the ZAMS mass comes from the difference in the assumed stellar evolution models. In the bottom left panel of Figure 2, we confirm that the numbers of BHs which contribute to BBH mergers do not exceed that expected from IMF.

In the following, we discuss the relation between the BH mass function (MF) obtained from IMF and the mass distribution of BHs contributed to merger events. The relation between the thermodynamical time (similar to merger timescale) and primary BH mass obtained from the results of  $N$ -body simulations is  $\tau \propto m_1$ . On the other hand, the BH MF obtained from IMF (see the left panels of Figure 2) follows  $dN/dm_{\text{BH}} \propto m_{\text{BH}}^{-1}$  for

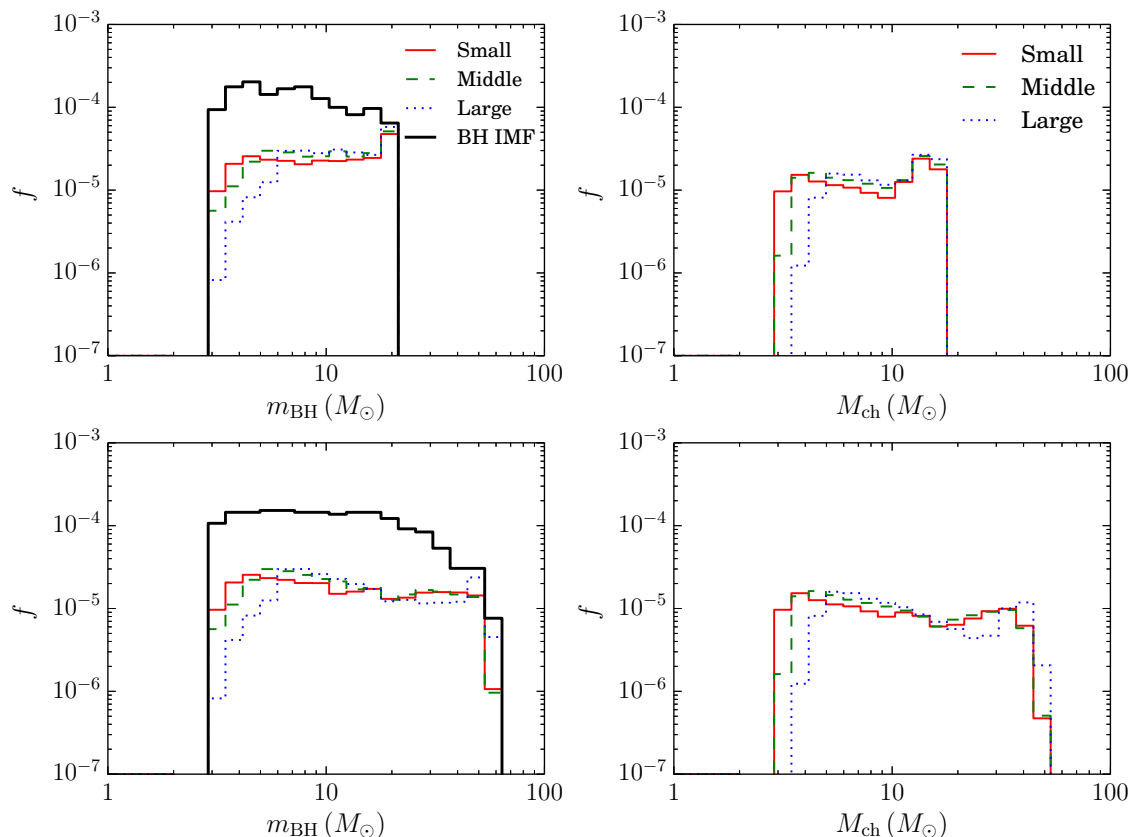


**Fig. 2.** Mass function of BHs which contribute to mergers for models small ( $N = 5 \times 10^5$ ), middle ( $N = 10^6$ ), and large ( $N = 2 \times 10^6$ ) of Tanikawa (2013) (top) and us (bottom). The fraction is normalized by the total number of cluster particles. Black histogram show the mass distribution of BHs obtained from the IMF and stellar evolution model. Right: normalized chirp mass distribution of merging BBHs for the models of Tanikawa (2013) (top) and us (bottom).

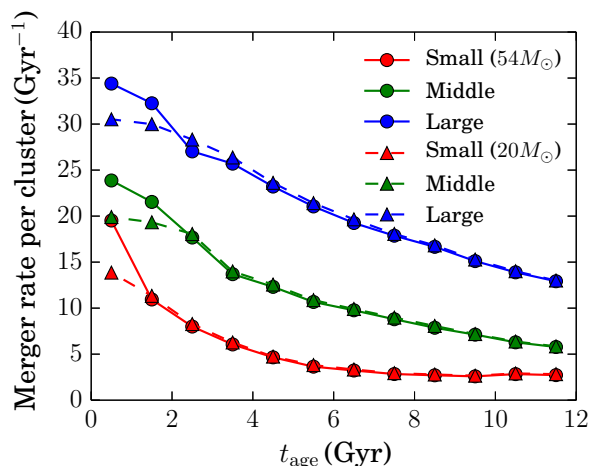


**Fig. 3.** Merger rate per cluster as a function of cluster age for models with a maximum mass for black holes of  $54M_\odot$  (dots and full curves) and  $20M_\odot$  (triangles and dashed curves).

the higher mass region. Combining these, we expect that the MF of BH mergers becomes almost flat at the high mass end. Indeed, we see almost flat distribution. The flat region becomes wider as the relaxation time decreases. In our models, model Small has the shortest relaxation time, and therefore it dynamically evolves most quickly. During the dynamical evolution of star clusters, the most massive BBHs selectively form and are ejected in the beginning, and then less massive BBHs start to be ejected. Therefore, the fraction of low-mass BBH mergers increases for clusters with a smaller  $N$ . Thus, our model reasonably reflects the dynamical evolution of star clusters and the distribution of BBHs formed there. We note that the cut-off mass at  $m_{\text{BH}} = 3M_\odot$  is adopted only in this paper, and therefore the BH mass distributions of this paper and Tanikawa (2013) are different at the low-mass end.

Natal kicks due to asymmetric supernova explosions also affect the merger rates of BBHs in star clusters because some BHs are ejected from their host star clusters due to the high-velocity kicks. The retention fraction is estimated to be 0.1 for neutron stars (Pfahl et al. 2002), but that of BHs depends on the fraction of fallback materials when they collapse, which affects the kick velocity (Fryer et al. 2012; Rodriguez et al. 2016). The fallback fraction increases as the BH mass increases, and as a



result the kick velocity decreases (Fryer et al. 2012). All BHs with a progenitor mass of  $> 40M_{\odot}$  are expected to retain in the cluster (Rodriguez et al. 2016). In Tanikawa (2013), the effect of natal kicks are included in their  $N$ -body simulations by a single retention fraction irrespective of stellar masses, and they found that the BBH merger rates are simply proportional to the retention fraction. From this result, the natal kicks do not seem to affect the dynamical evolution of star clusters. Therefore, we first assume that all BHs retain in star clusters and discuss the effect of natal kicks and retention rate in Section 4.1.

## 2.2 Cosmic star-cluster formation history

In order to estimate the BBH merger rate for the entire universe, we need the number density of globular clusters in the universe. In Tanikawa (2013), a single formation epoch for all globular cluster was assumed, but we adopt a number density of globular clusters as a function of redshift,  $z$ , (or universe age,  $t$ ). We assume that the star-cluster formation density is proportional to the star formation density of the universe (cosmic star formation history). Combining all survey data from ultraviolet to infrared, Madau & Dickinson (2014) obtained a cosmic star formation history as follows:

$$\psi(z) = 0.015 \frac{(1+z)^{2.7}}{1 + [(1+z)/2.9]^{5.6}} M_{\odot} \text{ year}^{-1} \text{ Mpc}^{-3}. \quad (13)$$

For the estimation of the number density of forming star clusters, we use the number of star clusters per stellar mass ( $10^9 M_{\odot}$ ),  $T$ , (Zepf & Ashman 1993) observationally determined for galaxies. We adopt  $T$  from the results of the Spitzer Survey of Stellar Structure in Galaxies ( $S^4G$ ) (Sheth et al. 2010), which includes both early- and late-type samples. According to their results,  $T$  depends on galaxy stellar mass ( $M_{\star}$ ):

$$T = \begin{cases} 10^{5.7} (M_{\star}/M_{\odot})^{-0.56} & (\text{for } 10^{8.5} < M_{\star} < 10^{10} M_{\odot}) \\ 8.3 & (\text{for } 10^{10} < M_{\star} < 10^{11} M_{\odot}) \\ 10^{-6.11} (M_{\star}/M_{\odot})^{0.63} & (\text{for } M_{\star} > 10^{11} M_{\odot}) \end{cases} \quad (14)$$

(Zaritsky et al. 2015, 2016).

Using these relation, the maximum and minimum number of star clusters per stellar mass of  $10^9 M_{\odot}$  are 87 for  $M_{\star} = 10^{8.5} M_{\odot}$  and 8.3 for  $M_{\star} = 10^{10.5} - 10^{11} M_{\odot}$ . In any cases,  $T \sim 10$ –100. We hereafter ignore the observed dependence of  $T$  on the mass of the host galaxy and adopt a fixed values of  $T = 10$  as our standard value.

In the top panel of figure 4, we show the number density of star clusters in comoving volume as a function of current age of star clusters ( $t_{GC,age}$ ). The distribution has a peak at  $t_{GC,age} \sim 9$  Gyr, and the number density drops for  $t_{GC,age} \gtrsim 10$  Gyr. We therefore ignore star clusters which are born more than 12 Gyr ago. In the bottom panel of figure 4, we show the total number density of clusters born before a certain look back time. The total number density of star clusters is  $7.8 \text{ Mpc}^{-3}$

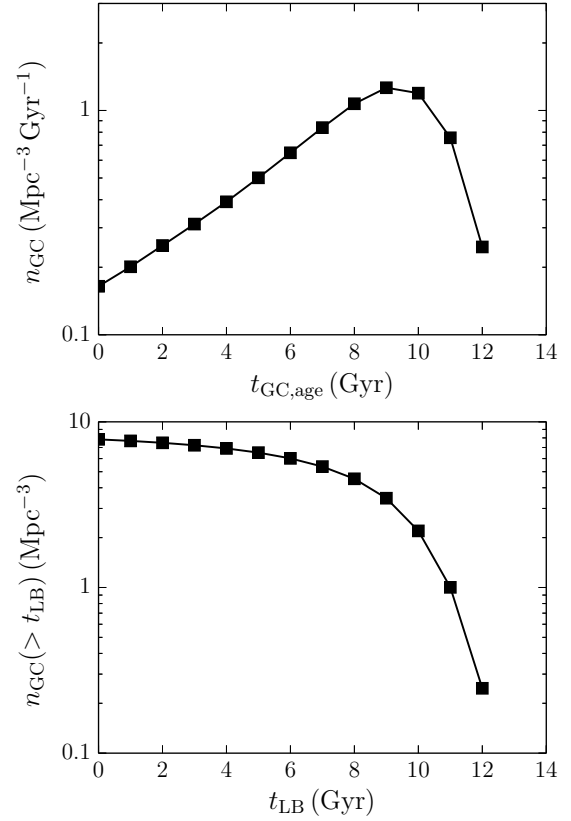


**Fig. 4.** The number density of star clusters in comoving volume as a function of cluster age (top) and the number density of globular clusters born before the lookback time (bottom). Here we adopt  $T = 10$ .

for  $T = 10$ . This value is a few times to an order of magnitude larger than those estimated in previous studies such as  $8.4h^3 \text{ Mpc}^{-3}$ , where  $h = H_0/100 \text{ km s}^{-1}$  (Portegies Zwart & McMillan 2000), and  $0.77 \text{ Mpc}^{-3}$  (Rodriguez et al. 2015). If we consider star clusters with the ages similar to those of globular clusters (clusters born before 10 Gyr), their number density is  $2.2 \text{ Mpc}^{-3}$  (see Figure 4), which is similar to the optimistic estimate in Rodriguez et al. (2015). Although most of massive clusters are globular clusters and they are old, in starburst galaxies and star-forming dwarf galaxies such as the Large and Small Magellanic Clouds, massive and dense star clusters, so-called super star clusters, are still forming (Portegies Zwart et al. 2010). They are dense and massive enough to form BBHs. We therefore estimate BBH merger rates both including and excluding star clusters younger than typical globular clusters in this study. We discuss the contribution of young star clusters to our final results in the following sections.

## 2.3 Initial mass function of star clusters

The mass function of merging BBHs and the merger rate depend on the total mass of star clusters ( $M_{cl}$ ). We therefore assume an initial mass function of globular clusters as  $dN_{cl}/dM_{cl} \propto M_{cl}^{-2}$

(Portegies Zwart et al. 2010), which is determined by the observations of young ( $< 1$  Gyr) star clusters in nearby galaxies. Although this relation is for young massive clusters in nearby galaxies, we assume that it is also applicable to globular clusters. Observed current globular cluster mass functions follows a lognormal distribution with a peak at  $\sim 2 \times 10^5 M_\odot$  (Brodie & Strader 2006; Jordán et al. 2007) rather than a power-law. This lognormal distribution is considered to be shaped from a power-law distribution due to the disruption of less massive clusters (Fall & Zhang 2001). On the other hand, Vesperini (2000) claimed that an initially lognormal distribution can reproduce the observations better than the power-law model. In both cases, star clusters less massive than the peak mass do not much contribute the total mass of star clusters. We therefore take into account only star clusters with  $\gtrsim 2 \times 10^5 M_\odot$ . We set the maximum mass of star clusters to be  $\sim 2 \times 10^6 M_\odot$ . If the cluster mass function is lognormal, the mass of the most massive cluster is a few times  $10^6 M_\odot$  (Jordán et al. 2007). The power of the observed young clusters is truncated at the high-mass end (Portegies Zwart et al. 2010). We adopt number fractions of our three cluster models as 0.57, 0.29, and 0.14 for models small, middle, and large, respectively. These fractions follows the power of  $-2$ . We assume that every 1 Gyr star clusters are born following the cosmic star-cluster formation history (see Figure 4) the number fractions.

## 2.4 BBH merger rates

Following Tanikawa (2013), we generate the distributions of 100 000 BBHs per cluster model using a Monte Carlo technique (see section 4.3 of Tanikawa 2013, for the details). Assuming  $n_{GC}(z)$  as described in the previous sections, we calculate BBH merger rates originating from star clusters in the universe as follows.

The cumulative merger rates up to a given  $z$  is calculated by integrating the merger rate for individual globular clusters at a given universe age ( $\Gamma_{\text{mrg}}(t)$ ) as:

$$\Gamma_{\text{mrg}}(< z) = \int_0^z \left[ n_{GC}(z') \frac{dV(z')}{dz'} \frac{\Gamma_{\text{mrg}}(z')}{1+z'} \right] dz', \quad (15)$$

where  $z$  is a function of  $t$  and  $1/[1+z(t)]$  is a factor coming from the cosmological time dilation of the merger rate. The volume,  $dV(z) = dV(t)$ , is expressed as:

$$dV(t) = 4\pi D_p(t)^2 dD_p(t), \quad (16)$$

where  $D_p(t)$  is a proper distance, which is obtained by

$$D_p(t) = c \int_t^{t_0} [1+z(t')] dt', \quad (17)$$

where  $c$  is the speed of light. The universe age,  $t$ , is written as

$$t = H_0^{-1} \int_z^\infty \frac{dz'}{(1+z') \sqrt{\Omega_m(1+z')^3 + \Omega_\Lambda}} \quad (18)$$

$$= \frac{1}{3H_0\sqrt{\Omega_\Lambda}} \log \left[ \frac{\sqrt{\Omega_m(1+z)^3 + \Omega_\Lambda} + \sqrt{\Omega_\Lambda}}{\sqrt{\Omega_m(1+z)^3 + \Omega_\Lambda} - \sqrt{\Omega_\Lambda}} \right] \quad (19)$$

We adopt the  $\Lambda$ CDM model with  $H_0 = 67.8 \text{ km s}^{-1} \text{ Mpc}^{-1}$ ,  $\Omega_m = 0.308$ ,  $\Omega_\Lambda = 0.692$ , and  $\Omega_k = 0.0$  from Planck 2015 results (Planck Collaboration et al. 2015).

We obtain  $\Gamma_{\text{mrg}}(t)$  from the models based on the  $N$ -body simulations described in Section 2.1 and  $n_{GC}(t)$  from the cosmic star formation history as described in Section 2.2. We show the cumulative merger event rate obtained from equation (15) and the sub-fractions depending on chirp mass and redshifted chirp mass in the left panels of Figure 5. The merger rates reach to more than  $10^4 \text{ yr}^{-1}$ , but not all of them are observable. Most of star clusters were born 9–12 Gyr ago and their dynamical activity decreases with time. Therefore, the majority of BBH mergers occur at high- $z$ , for which LIGO sensitivity is not sufficient.

We also present the merger rate density in the local universe ( $z < 0.1$ ) in the right panels of Figure 5. In the local universe, the BBH merger rate density is estimated to be  $57 \text{ Gpc}^{-3} \text{ yr}^{-1}$ , which is consistent with the value estimated from LIGO observation,  $9\text{--}240 \text{ Gpc}^{-3} \text{ yr}^{-1}$  (The LIGO Scientific Collaboration et al. 2016). If we allow the formation of star clusters which can form merging BBHs only in the earlier universe ( $> 10$  Gyr ago), the fraction of massive BBHs significantly decreases because massive BBH mergers in the local universe originates from younger star clusters in our models. The merger rate density decreases down to  $13 \text{ Gpc}^{-3} \text{ yr}^{-1}$  if we assume that only old clusters which were born 10–12 Gyr ago can be the source of BBH mergers. However, the merger rate is still within the observational estimates.

Rodriguez et al. (2016) estimated merger rates originating from BBHs formed in star clusters using the results of Monte-Carlo simulations of globular clusters and obtained a merger rate of  $\sim 5 \text{ Gpc}^{-3} \text{ yr}^{-1}$  from their standard model. Park et al. (2017) also estimated a similar merger rate density ( $6.5 \text{ Gpc}^{-3} \text{ yr}^{-1}$ ) using direct  $N$ -body simulations of star clusters with  $5 \times 10^4$  particles. These values are an order of magnitude lower than ours. One possible reason is that while we take all star clusters to  $z = 0$  into account, they assumed that only globular clusters form BBHs. Therefore, the total number density of star clusters in our model is an order of magnitude higher than their model (see Section 2.2 for the details).

In the left panel of Figure 6, we present the redshifted chirp mass distribution of BBH mergers originating from star clusters. Including all star clusters, we obtain a weak double-peak distribution of redshifted chirp mass. If we exclude young clusters, the merger rates slightly decrease, but do not change much because most of clusters were born 10–12 Gyr ago. In the right panel of Figure 6, we present the merger rate density in the local universe ( $z < 0.1$ ) for comparison with the results of common

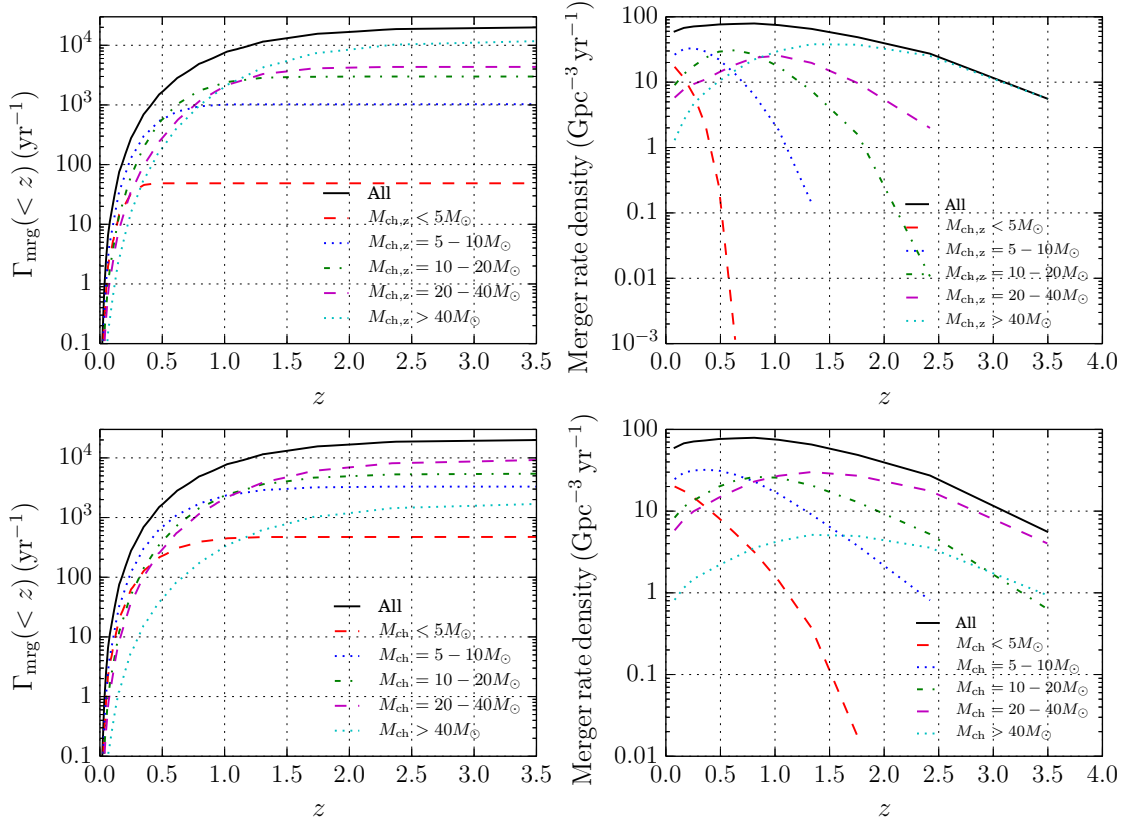


**Fig. 5.** Cumulative merger rates (left) and merger rate densities (right). Top and bottom panels are with subsets of redshifted chirp mass and chirp mass, respectively.

envelope evolution model (Belczynski et al. 2016). We here see double-peak distributions. The high-mass peak is located at  $M_{\text{chirp},z} \sim 40\text{--}50M_{\odot}$ . On the other hand, the peak is the total redshifted mass of  $\sim 30\text{--}40M_{\odot}$  in the case of common envelope model (see Figure 3 in Belczynski et al. 2016). If we assume equal-mass binaries, it corresponds to  $M_{\text{chirp},z} \sim 20M_{\odot}$ . The low-mass peak in the redshifted chirp mass function is at  $5\text{--}7M_{\odot}$ . The high-mass peak becomes weaker, if we limit the cluster formation epoch to higher- $z$ .

## 2.5 Detectability

In order to calculate the detection rate, we have to consider the detectability of each merger event. We follow Tanikawa (2013) (see also O’Leary et al. 2006) and assume that BBH mergers are detected when the merger events satisfy:

$$C_{\text{det}} = \left( \frac{D_L}{D_{L,0}} \right)^{-1} \left( \frac{M_{\text{ch},z}}{M_{\text{ch},0}} \right)^{5/6} \left[ \frac{s(f_{\text{off}})}{s(f_{\text{off},0})} \right]^{1/2} > 1, \quad (20)$$

where  $D_L (= [1 + z(t)]D_p(t))$  is a luminosity distance,  $M_{\text{ch},z}$  is a redshifted chirp mass, and  $s(f_{\text{off}})$  is a detector response function. The redshifted chirp mass is written as

$$M_{\text{ch},z} = [1 + z(t)]M_{\text{ch}}, \quad (21)$$

where  $M_{\text{ch}}$  is a chirp mass of a binary with masses of  $m_1$  and  $m_2$ , which is given by

$$M_{\text{ch}} = \frac{(m_1 m_2)^{3/5}}{(m_1 + m_2)^{1/5}}. \quad (22)$$

The detector response function is approximated as

$$s(f_{\text{off}}) = \int_0^{f_{\text{off}}} \frac{(f')^{-7/3}}{S_N(f')} df', \quad (23)$$

where  $S_N(f)$  is the noise spectral density and  $f_{\text{off}}$  is the cutoff frequency (Cutler & Flanagan 1994).

Instead of using  $S_N(f)$  and  $f_{\text{off}}$  adopted in Tanikawa (2013), we adopt the following functions. For  $S_N(f)$ , we perform a least square fitting to the latest sensitivity spectrum of aLIGO-Hanford on October 1, 2015 (Kissel 2015). The fitted sensitivity spectrum is given by

$$\log(\text{Strain}) = -24 + 4.4[\log(f)]^{-3.0} + 0.034[\log(f)]^{3.1} \quad (24)$$

and shown in Figure 7. We note that  $S_N(f) = (\text{Strain})^2$ . We also perform a fitting to the final design spectrum (Abbott et al. 2016c) and obtain

$$\log(\text{Strain}) = -24 + 2.2[\log(f)]^{-2.3} + 0.011[\log(f)]^{3.7}. \quad (25)$$

This function is also shown in Figure 7. We adopt this only for  $D_{L,0} = 200$  Mpc. For  $f_{\text{off}}$ , we adopt the ringdown frequency



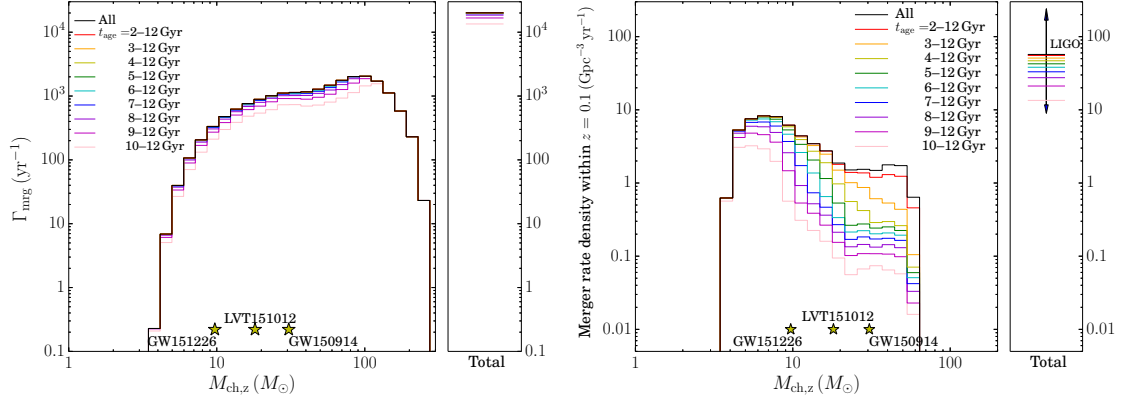


**Fig. 6.** The merger rate distribution as a function of redshifted chirp mass and the total merger rates for all BBH mergers (left) and merger rate density distribution as a function of redshifted chirp mass and the total merger rate density for mergers within  $z = 0.1$  (right). Black arrow indicate in the right panel indicate the range of the merger rate density estimated by LIGO observation (The LIGO Scientific Collaboration et al. 2016).

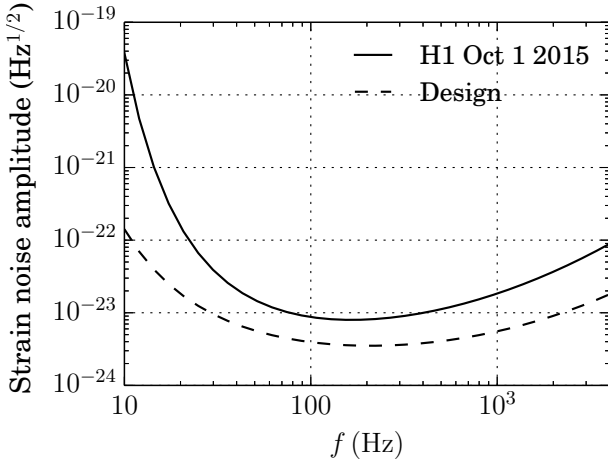


**Fig. 7.** Sensitivity spectrum obtained from LIGO H1 on Oct 1 2015 (LIGO-G1501223) (Kissel 2015) and the design sensitivity spectrum (Abbott et al. 2016c).

expressed as:

$$f_{\text{off}} = \frac{c^3}{3\pi G M_f} [1.5251 - 1.1568(1 - a_f)^{0.1292}], \quad (26)$$

where  $M_f$  and  $a_f$  is the final mass and spin of the merger remnant (Berti et al. 2006; Haster et al. 2016). We assume  $a_f = 1$  and  $M_f = M_{f,\text{max}} = 0.89(m_1 + m_2)$  (Healy et al. 2014).

For  $M_{\text{ch},0}$  and  $f_{\text{off},0}$ , we adopt the chirp mass and cut-off frequency for an NS-NS merger with a mass of  $1.4M_\odot$ , which are  $1.2M_\odot$  and 4800 Hz, respectively. Here,  $D_{L,0}$  is the detection limit in luminosity distance for a NS-NS merger. We adopt  $D_{L,0} = 40, 80, 120$ , and 200 Mpc, which correspond to the detectable range for the current and future observations. The detectable range for NS-NS mergers is expected to be 40–80 Mpc for the observation in 2015–16, 80–120 Mpc in 2016–2017, 120–170 Mpc in 2017–18, and 200 Mpc for the full sensitivity in 2019. The signal-to-noise ratio (SNR) for detection is assumed to be 8 (Abbott et al. 2016c). Using our description,

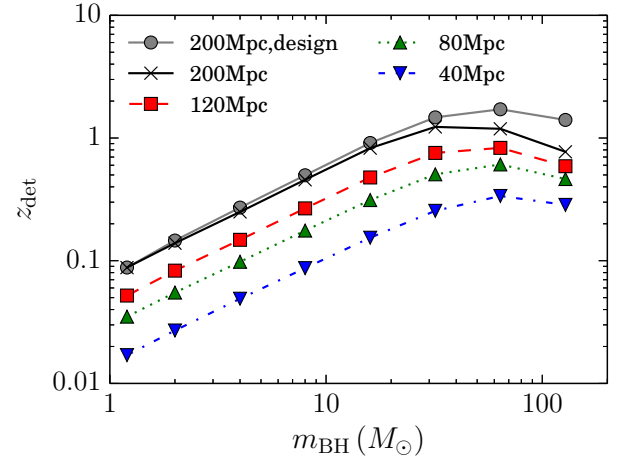


**Fig. 8.** The detection limit as a function of the mass of a BH for  $D_{L,0} = 200, 120, 80$ , and 40 and for each sensitivity spectrum. Here we assume that BBHs are equal mass systems. The smallest value of  $m_{\text{BH}}$  corresponds to  $1.2M_\odot$ .

the cut-off frequency and the SNR of GW150914 are calculated as 190 Hz and 21, respectively, assuming  $D_{L,0} = 80\text{Mpc}$ ,  $z = 0.09$ , and the black hole masses are 36 and  $29M_\odot$  (Abbott et al. 2016b). These values are consistent with the actual observation.

In Figure 8, we present the maximum detectable redshift ( $z_{\text{det}}$ ) as a function of the mass of NSs or BHs ( $m_{\text{BH}}$ ) for each  $D_{L,0}$  and sensitivity spectrum. Here we assume that the BBHs are equal mass systems and that  $\text{SNR} > 8$  for the detection. These results are roughly consistent with obtained in other works (e.g., see Figure 4 in Abbott et al. 2016a).

We calculated the cumulative detection rate up to  $z$  as

$$\Gamma_{\text{det}}(< z) = f_{\text{det}}^{-3} \int_0^z \left[ n_{\text{GC}}(z') \frac{dV(z')}{dz'} \frac{\Gamma_{\text{det}}(z')}{1 + z'} \right] dz', \quad (27)$$

where  $f_{\text{det}} = 2.26$  is a factor for the non-uniform pattern of detector sensitivity and random sky orientation of sources (Finn

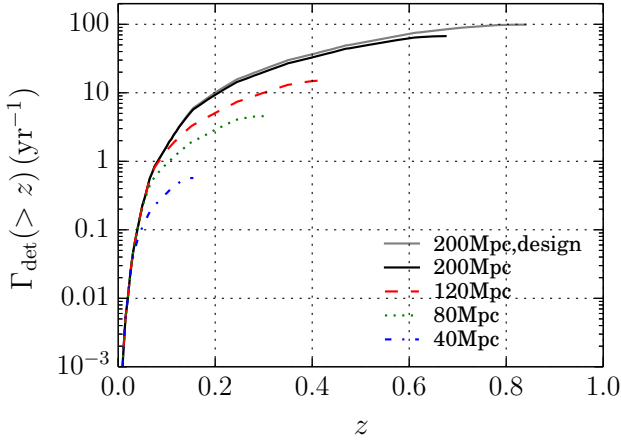


**Fig. 9.** Cumulative detection rate per year within redshift  $z$  for  $D_{L,0} = 200$ , 120, 80, and 40 and for each sensitivity spectrum.

& Chernoff 1993), and  $\Gamma_{\text{det}}(z')$  is the detection rate at  $z'$ , which is the rate of mergers satisfying  $C_{\text{det}} > 1$ .

We estimate the detection rates of BBH mergers by aLIGO, using models for the distribution of BBHs based on direct  $N$ -body simulations (Tanikawa 2013), cosmic star-cluster formation history, and the detection model described in this section. We first generate BBH merger history per cluster using the models of Tanikawa (2013). Following the cosmic star-cluster formation rate, we assume that star clusters form every 1 Gyr. From these, we calculate the merger rate of BBHs in the universe and their mass distribution. Assuming the detection model as is described in this section, we further calculate the detection rates of BBHs and their mass distribution. We performed these calculations using Python scripts working on AMUSE (the Astrophysical Multipurpose Software Environment) framework (Portegies Zwart et al. 2009; Pelupessy et al. 2013).

### 3 Results: Detection rates

In Figure 9, we present the cumulative detection rate of BBH mergers as a function of redshift ( $z$ ) obtained from our models. The total detection rates are 67, 15, 4.6, and 0.57 per year for  $D_{L,0}=200$ , 120, 80, and 40 Mpc, respectively, assuming the sensitivity spectrum on Oct 1 in 2015 and  $T = 10$ . Even for the current detection limit ( $\sim 70$  Mpc) (Kissel 2015), the detection rate reaches several per year. Here, we assume that massive star clusters continue to form to  $z = 0$  following the cosmic star cluster formation history. With the final design sensitivity spectrum, the total detection rate increases to 99 per year for  $D_{L,0} = 200$  Mpc. If we assume a larger value for  $T$ , the detection rate increases.

We present the redshifted chirp mass function of the detected BBH mergers in Figure 10. The mass function has a peak at  $M_{\text{ch},z} \sim 60\text{--}80 M_{\odot}$  slightly depending on the values of  $D_{L,0}$ .

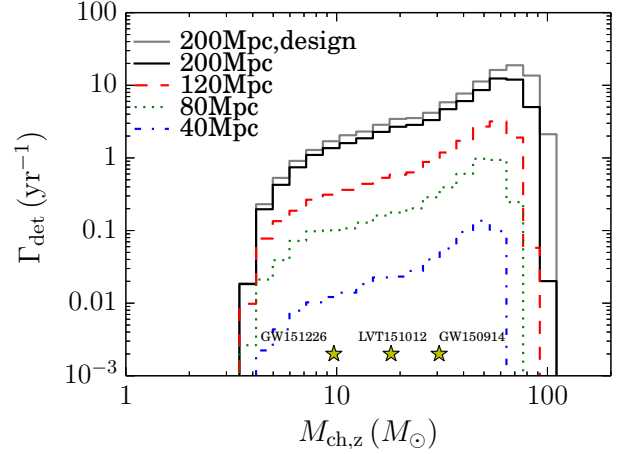


**Fig. 10.** Redshifted chirp mass distribution of detected merging BBHs for the detection range ( $D_{L,0}$ ) of 200, 120, 80, and 40 Mpc (black full, red dashed, green dotted, and blue dash-dotted lines), respectively. Gray full line indicate  $D_{L,0} = 200$  Mpc, but for the final design sensitivity spectrum (see Figure 7) Note that  $D_{L,0} = 80$  Mpc corresponds to the sensitivity of current aLIGO. Stars indicate the mass of detected BBH mergers (The LIGO Scientific Collaboration et al. 2016).

The merger rates of the intermediate mass range of the BBHs ( $M_{\text{ch},z} \sim 10\text{--}30$ ) is almost flat. We also plot the mass of the detected BBH mergers with redshifted chirp masses of 31, 9.7, and 18 for GW150914, GW151226, and LVT151012, respectively (The LIGO Scientific Collaboration et al. 2016). They are located in this flat region.

Figure 11 shows the changes in detection rates when we limit the formation epoch of star clusters. The left and right panels are for the cases of current aLIGO detection limit ( $D_{L,0} = 80$  Mpc) and future detection limit ( $D_{L,0} = 200$  Mpc), respectively. Black curves correspond to the detection rates shown in Figure 10. If we consider star clusters older than 10 Gyr, the detection rates decrease down to 0.23 and 5.1 per year for the current and future detection limits, respectively. Not only the detection rates, the shapes of the redshifted chirp-mass function also changes. The detection rates of higher-mass BBH mergers significantly decreases and the shape of the mass function becomes double-peaked, because massive BBH mergers originating from younger star clusters are excluded. The low-mass peak is located at  $7\text{--}8 M_{\odot}$ . We summarize the merger rate density and detection rates for the current and future detection limits of LIGO in Table 2.

In Figure 12, we also present the distribution of BH mass ratio ( $q$ ) of detected BBH mergers. The distribution of  $q$  does not depend on the detectable distances. We therefore plot it only for models with  $D_{L,0} = 200$  Mpc and the designed sensitivity and current aLIGO ( $D_{L,0} = 80$  Mpc). We also plot the distribution of  $q$  for all merger events occurred until the current age of the universe and confirmed that this distribution of  $q$  is caused by the dependence of  $t_{\text{GW}}$  on  $q$ . BBHs with a higher eccen-

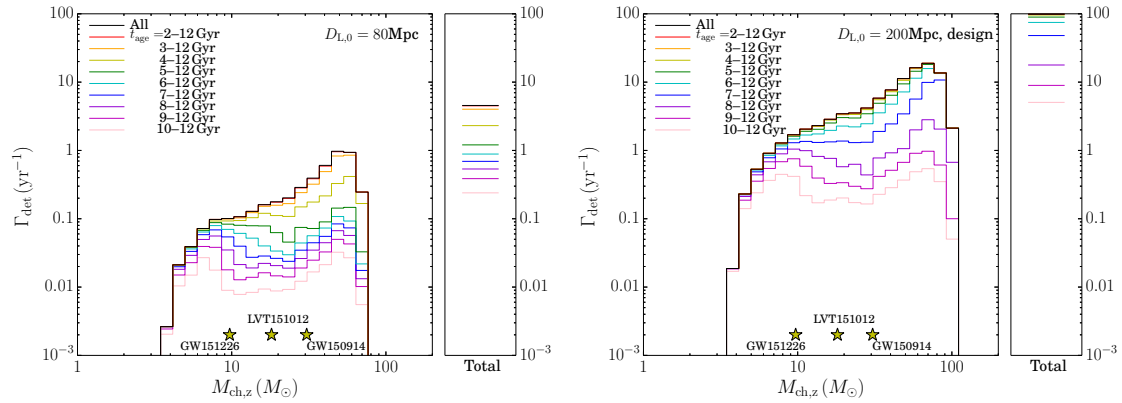


**Fig. 11.** Redshifted chirp mass distribution of detected merging BBHs for the ranges of cluster formation for the current detection limit of aLIGO (left) and future detection limit (right).

tricity have a shorter  $t_{\text{GW}}$ , and therefore the  $q$ -distribution of merging BBHs are more dominated by eccentric binaries compared to the initial distribution. The distribution of the mass ratio predicted by common envelope scenario, which depends on the initial distribution of binary mass ratio and the metallicity, has a much steeper dependence on the mass ratio (Belczynski et al. 2014; Dominik et al. 2015), although this may be because they assumed a flat initial mass ratio ( $q \sim 1$  for most of massive stars) distribution. Even if primordial binaries in star clusters have the same initial mass ratio, the mass ratio would change due to the dynamical evolution in star clusters. Thus, we can probably regard the shapes of BBH mass function and the mass ratio as the signature of the dynamical formation of BBHs in star clusters and expect that observations of a large number of BBH mergers in the near future will tell us the formation mechanisms of merging BBHs.

## 4 Discussion

### 4.1 Natal kicks

BHs receive natal kicks when they form because of asymmetric supernova explosions. The kick velocities can exceed escape velocities of star clusters, and as a consequence the kicked BHs can be ejected from the host star clusters. The observation of radio pulsars suggests the one-dimensional velocity dispersion of  $265 \text{ km s}^{-1}$  (Hobbs et al. 2005), which is much larger than typical escape velocities. On the other hand, recent stellar evolution models suggest that the kick velocity depends on the fraction of fallback materials when they explode and that massive BHs formed via direct collapse do not receive any kicks (Belczynski et al. 2006; Fryer et al. 2012).

Tanikawa (2013) performed direct  $N$ -body simulations assuming a constant retention fraction between 0.25 and 1.0 irrespective of BH masses and found that the BBH merger rates are proportional to the retention fraction. In this section, we

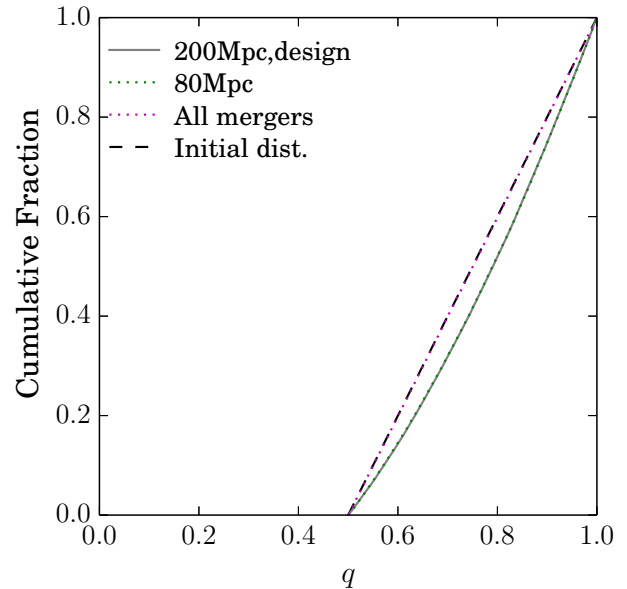


**Fig. 12.** Cumulative distribution of BH mass ratio of detected BBH mergers for models with  $D_{L,0} = 200 \text{ Mpc}$  and  $D_{L,0} = 80 \text{ Mpc}$ , all merger events, and the initial distribution (see equation (4))

estimate the merger and detection rates of BBHs assuming that BBH merger rate is proportional to the retention fraction and that the retention fraction depends on BH masses. For simplicity, we assume that the retention fraction linearly changes from 0.1 for  $M_{\text{BH}} = 3M_{\odot}$  to 1.0 for  $M_{\text{BH}} = 20M_{\odot}$  and that all BHs with  $M_{\text{BH}} > 20M_{\odot}$  remain in the clusters. The minimum BH mass for the direct collapse depends on metallicity and  $M_{\text{BH}} > 15\text{--}30M_{\odot}$  for  $Z = 0.01Z_{\odot}$ , where  $Z_{\odot}$  is the solar metallicity, is suggested (Belczynski et al. 2016).

In Figure 13, we present the merger rate of all mergers and merger rate density for the local universe ( $z < 0.1$ ) as a function of redshifted chirp mass. Compared with the case without kicks (see Figure 6), the fraction of low-mass BHs signifi-

**Table 2.** Summary of the results

Model		Merger rate density ( $z < 0.1$ ) ( $\text{Gpc}^{-3} \text{yr}^{-1}$ )	Detection rate	
			Current ( $\text{yr}^{-1}$ )	Future ( $\text{yr}^{-1}$ )
$M_{\text{BH,max}} = 54M_{\odot}$	$t_{\text{age}} = \text{all}$	57	4.6	99
	$t_{\text{age}} = 10\text{--}12 \text{ Gyr}$	13	0.23	5.1
	$t_{\text{age}} = \text{all, with natal kick}$	16	3.9	86
	$t_{\text{age}} = 10\text{--}12 \text{ Gyr, with natal kick}$	1.3	0.14	2.9
$M_{\text{BH,max}} = 20M_{\odot}$	$t_{\text{age}} = \text{all}$	57	1.8	37
	$t_{\text{age}} = 10\text{--}12 \text{ Gyr}$	14	0.17	3.7

$M_{\text{BH,max}}$  is the maximum mass of BHs.  $t_{\text{age}}$  indicates the range of cluster age we included. Current and future detection rates indicate the detection rate for  $D_{\text{L},0} = 80$  and 200 Mpc, respectively.

cantly decreases, and the total merger rates also decrease. The total retention fraction of BHs obtained from our assumption is  $\sim 0.7$ , which is consistent with retention fractions of 0.4–0.7 obtained from models of kick velocities depending on BH masses (the amount of fallback materials) (Belczynski et al. 2006; Portegies Zwart et al. 2007). The merger rate density within  $z = 0.1$  including young star clusters born down to  $z = 0$  is  $16 \text{ Gpc}^{-3} \text{yr}^{-1}$ , which is still within the range estimated by LIGO (The LIGO Scientific Collaboration et al. 2016). If young star clusters are excluded, the merger rate density drops to  $1.3 \text{ Gpc}^{-3} \text{yr}^{-1}$ . The results with natal kicks are also summarized in Table 2.

Figure 14 shows the distribution of detection rates as a function of redshifted chirp mass expected from our natal-kick model. The estimated detection rates are 0.14–3.9 per year for the current detection limit ( $D_{\text{L},0} = 80 \text{ Mpc}$ ) 2.9–86 per year for the future detection limit ( $D_{\text{L},0} = 200 \text{ Mpc}$ ). In the case without natal kicks, the distribution of detection rates show a peak close to the high-mass end, and another peak appears when younger clusters are ignored (see Figure 11). With natal kicks, however, the detection rate always show a strong peak at the high-mass end.

## 4.2 Metallicity evolution and BH mass function

Another important parameter we had not accounted for is the change of the metallicity of star clusters as a function of  $z$  and the resulting BH mass function. The metallicity strongly affect the stellar evolution and the final BH masses. Stars with lower metallicity can form more massive BHs. Recent stellar evolution models suggest that the maximum BH mass reaches  $\sim 100M_{\odot}$  for  $Z = 0.0001$ , but only  $\sim 15M_{\odot}$  for the solar metallicity (Belczynski et al. 2016). The mean metallicity of the universe increases with time (Madau & Dickinson 2014). The maximum mass of BHs, therefore, should decrease as the formation epoch of the host star clusters delays. Furthermore, the metallicity of star clusters born in the same redshift should have a dispersion. In the local universe, starburst galaxies which are still forming massive star clusters, such as the Large and Small Magellanic Clouds, have a metallicity lower than the av-

erage ( $\sim 0.4$  and  $\sim 0.2$ , respectively) (Cole et al. 2005; Luck et al. 1998). Recent stellar evolution models expected that BHs with a maximum mass of  $\sim 30M_{\odot}$  (Belczynski et al. 2016) may form in the Magellanic Clouds. In addition, the natal kick velocity also decreases as the metallicity decreases (Belczynski et al. 2016). Thus, evolution models of the mean metallicity with a dispersion should be included, but has not fully been done yet for star cluster models. Rodriguez et al. (2016) recently performed a series of Monte-Carlo simulations of star clusters for three different metallicity (0.01, 0.05, and  $0.025 Z_{\odot}$ ) with recent prescriptions of stellar evolution and natal kicks. They estimated BBH merger rates, but they assumed all star clusters were born 12 Gyr ago.

Since the metallicity affects the stellar evolution and kick velocity, the dynamical evolution of star clusters may be affected. In some cases, however, the effects on the dynamical evolution is suggested to be limited due to the small fraction of massive stars (Tanikawa 2013), although we still need to investigate the effect by performing direct  $N$ -body simulations changing the metallicity and related stellar evolution models. Such simulations consume a large amount of computational resources. We therefore do not perform additional direct  $N$ -body simulations here, but test a model with a smaller upper-mass limit of BH mass based on the model of Tanikawa (2013).

Instead of considering a cosmic metallicity evolution and the dispersion, we perform the same analyses for a model with a maximum BH mass of  $20M_{\odot}$ , which is obtained from the direct  $N$ -body simulations of Tanikawa (2013) and compare the results to the cases with a maximum BH mass of  $54M_{\odot}$ . In Figure 15, we present the merger rate of all mergers and merger rate density for  $z < 0.1$  as a function of redshifted chirp mass. Since there is no massive BHs than  $20M_{\odot}$ , no GW150914-like BBH merger occurs. The shape of mass functions are similar to those for a model with  $m_{\text{BH,max}} = 54M_{\odot}$ , and the merger rate densities within  $z = 0.1$  are  $14\text{--}57 \text{ Gpc}^{-3} \text{yr}^{-1}$  changing the ranges of cluster formation epoch.

In Figure 16, we present the distribution of detection rate as a function of redshifted chirp mass. The detection rates are 0.22, 1.8, 6.0, 29, and  $37 \text{ yr}^{-1}$  for  $D_{\text{L},0} = 40, 80, 120, 200 \text{ Mpc}$  and 200 Mpc with designed sensitivity, respectively. These re-

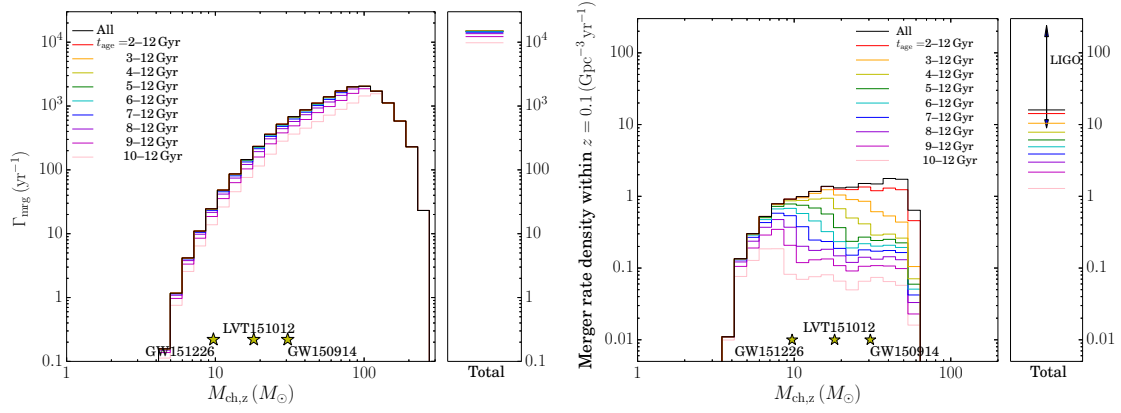


Fig. 13. Same as Figure 6, but with the natal-kick model.

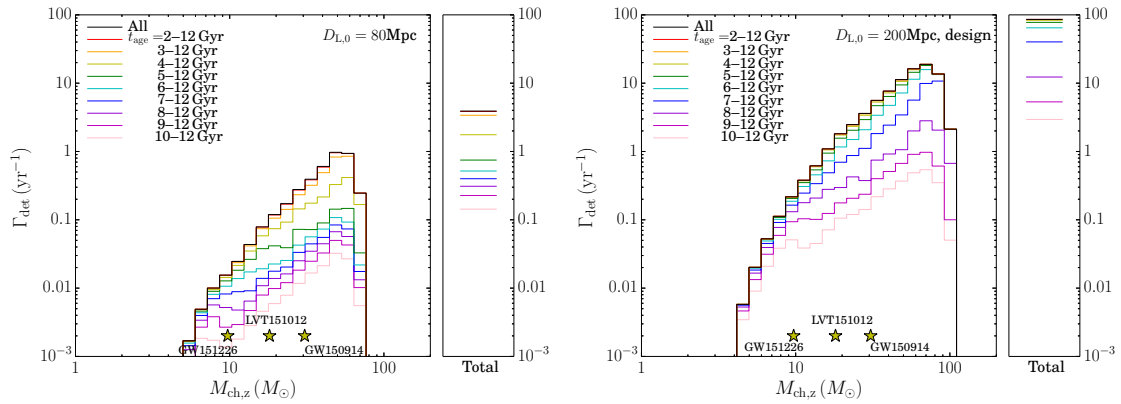


Fig. 14. Same as Figure 11, but with the natal-kick model.

sults are summarized in Table 2. Compared with the results of Tanikawa (2013), our model enhances massive BBH mergers. While Tanikawa (2013) assumed star cluster formation at 10 or 12 Gyr ago, we adopt a star-cluster formation history including younger star clusters. Since more massive BBHs merge more frequently in younger ages of star clusters, most of massive BBH mergers occur at high  $z$  and thus are unreachable with current or future LIGO, if we assume single cluster formation event at  $> 10$  Gyr ago. Our redshifted chirp mass function, therefore, contains massive BBH mergers more than that of Tanikawa (2013). We also updated the detection criterion using the recent model of the LIGO sensitivity. This also changed the shape of mass function of detected BBHs from that of Tanikawa (2013).

## 5 Summary

We estimated the BBH merger rates and the detection rates originating from the dynamical evolution of star clusters using a model of BBH-merger distribution obtained from  $N$ -body simulations performed by Tanikawa (2013). We assumed that globular clusters were born following the cosmic star formation rate.

Combining the BBH merger history per cluster and the cosmic star-cluster formation history, we obtained the merger rate density in the local universe ( $z < 0.1$ ) of  $57 \text{ Gpc}^{-3} \text{ yr}^{-1}$  including young star clusters and  $13 \text{ Gpc}^{-3} \text{ yr}^{-1}$  taking old globular clusters born 10–12 Gyr ago into account. These values are consistent with the values estimated from LIGO ( $9\text{--}240 \text{ Gpc}^{-3} \text{ yr}^{-1}$ , The LIGO Scientific Collaboration et al. 2016). We also estimated the detection rates of BBH merger events as 67, 15, 4.6, and 0.67 per year for  $D_{L,0}=200, 120, 80$ , and 40 Mpc, respectively, assuming the sensitivity spectrum on Oct 1 in 2015 and including young star clusters. For the final design sensitivity spectrum, the total detection rate increases to 99 per year for  $D_{L,0} = 200$  Mpc. If we assume that only star clusters born in a higher redshift can form BBHs, this value drops to  $\sim 5$  per year. In addition, if we assume that less massive BHs are ejected due to the natal kicks, it decreases down to  $\sim 3$  per year. Taking natal kicks into account, the merger rate density in the local universe is estimated to be 1.3 and  $16 \text{ Gpc}^{-3} \text{ yr}^{-1}$  excluding and including young star clusters, respectively.

We also predicted the redshifted chirp mass distribution of detected BBH mergers. The mass function of detected BBH mergers dynamically formed in star clusters has a peak at its



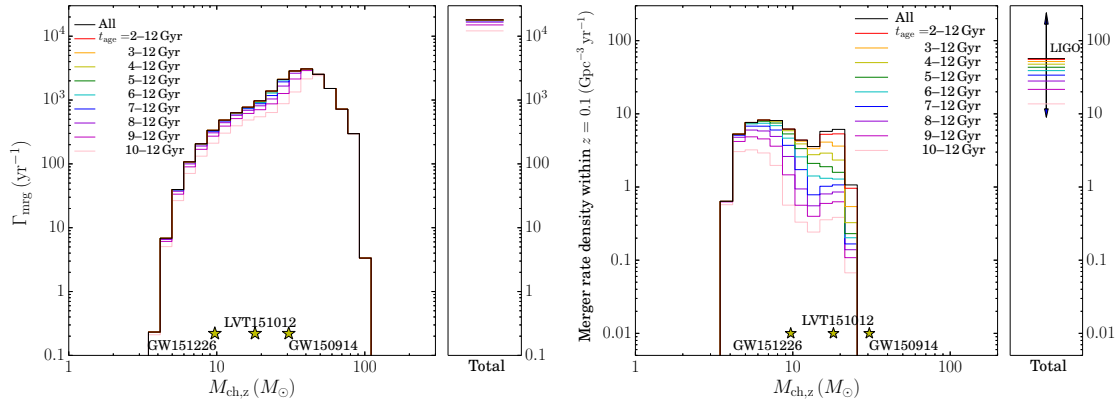


Fig. 15. Same as Figure 6, but for a model with a maximum BH mass of  $20M_{\odot}$ .

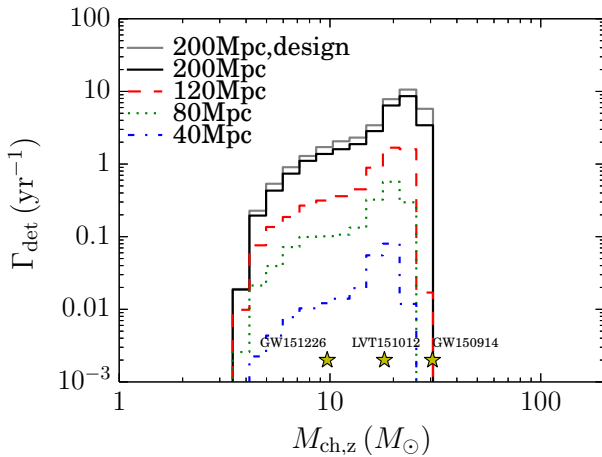


Fig. 16. Same as Figure 10, but for  $m_{\text{BH,max}} = 20M_{\odot}$ .

high-mass end, if we account for all star clusters born down to  $z = 0$ . The detection rate in the intermediate mass range is almost flat. If we assume that only star clusters born in a higher redshift can form BBHs, the mass distribution changes to a double-peaked shape with a low-mass peak at  $7\text{--}8M_{\odot}$ . The high-mass peak is not because of the initial mass function of BHs, but because of the dynamical evolution of star clusters and the typical lifetime of BBHs after their formation in star clusters. In dense star clusters, massive BHs selectively form binaries, and their separations shrink via three-body encounters. Thus, a mass distribution with a peak at its high-mass end is a typical signature of the dynamically formed BBHs and is also predicted by similar studies (e.g., Rodriguez et al. 2016).

## Acknowledgments

We thank the anonymous referee for the useful comments. This work was supported by JSPS KAKENHI Grant Number 26800108 and 17H06360.

## References

- Aarseth S. J., 2003, *Gravitational N-Body Simulations*. p. 430
- Abadie J., Abbott B. P., Abbott R., Abernathy M., Accadia T., Acernese F., Adams C., Adhikari R., Ajith P., Allen B., et al., 2010, *Classical and Quantum Gravity*, 27, 173001
- Abbott B. P., Abbott R., Abbott T. D., Abernathy M. R., Acernese F., Ackley K., Adams C., Adams T., Addesso P., Adhikari R. X., et al., 2016a, *ApJL*, 818, L22
- , 2016b, *Physical Review Letters*, 116, 061102
- , 2016c, *Living Reviews in Relativity*, 19
- Bae Y.-B., Kim C., Lee H. M., 2014, *MNRAS*, 440, 2714
- Banerjee S., Baumgardt H., Kroupa P., 2010, *MNRAS*, 402, 371
- Belczynski K., Bulik T., Fryer C. L., Ruiter A., Valsecchi F., Vink J. S., Hurley J. R., 2010, *ApJ*, 714, 1217
- Belczynski K., Buonanno A., Cantiello M., Fryer C. L., Holz D. E., Mandel I., Miller M. C., Walczak M., 2014, *ApJ*, 789, 120
- Belczynski K., Holz D. E., Bulik T., O’Shaughnessy R., 2016, *Nature*, 534, 512
- Belczynski K., Sadowski A., Rasio F. A., Bulik T., 2006, *ApJ*, 650, 303
- Belczynski K., Taam R. E., Kalogera V., Rasio F. A., Bulik T., 2007, *ApJ*, 662, 504
- Berti E., Cardoso V., Will C. M., 2006, *Phys. Rev. D*, 73, 064030
- Brodie J. P., Strader J., 2006, *ARA&A*, 44, 193
- Cole A. A., Tolstoy E., Gallagher III J. S., Smecker-Hane T. A., 2005, *AJ*, 129, 1465
- Cutler C., Flanagan É. E., 1994, *Phys. Rev. D*, 49, 2658
- Dominik M., Berti E., O’Shaughnessy R., Mandel I., Belczynski K., Fryer C., Holz D. E., Bulik T., Pannarale F., 2015, *ApJ*, 806, 263
- Downing J. M. B., Benacquista M. J., Giersz M., Spurzem R., 2011, *MNRAS*, 416, 133
- Eldridge J. J., Tout C. A., 2004, *MNRAS*, 353, 87
- Fall S. M., Zhang Q., 2001, *ApJ*, 561, 751
- Farrell S. A., Webb N. A., Barret D., Godet O., Rodrigues J. M., 2009, *Nature*, 460, 73
- Finn L. S., Chernoff D. F., 1993, *Phys. Rev. D*, 47, 2198
- Fryer C. L., Belczynski K., Wiktorowicz G., Dominik M., Kalogera V., Holz D. E., 2012, *ApJ*, 749, 91
- Giersz M., Hoggie D. C., 2009, *MNRAS*, 395, 1173
- , 2011, *MNRAS*, 410, 2698
- Haster C.-J., Wang Z., Berry C. P. L., Stevenson S., Veitch J., Mandel I., 2016, *MNRAS*, 457, 4499

- Healy J., Lousto C. O., Zlochower Y., 2014, *Phys. Rev. D*, 90, 104004
- Heggie D. C., Giersz M., 2008, *MNRAS*, 389, 1858
- Hobbs G., Lorimer D. R., Lyne A. G., Kramer M., 2005, *MNRAS*, 360, 974
- Hurley J. R., Pols O. R., Tout C. A., 2000, *MNRAS*, 315, 543
- Hurley J. R., Tout C. A., Aarseth S. J., Pols O. R., 2001, *MNRAS*, 323, 630
- Jordán A., McLaughlin D. E., Côté P., Ferrarese L., Peng E. W., Mei S., Villegas D., Merritt D., Tonry J. L., West M. J., 2007, *ApJS*, 171, 101
- King I. R., 1966, *AJ*, 71, 64
- Kissel J., 2015, LIGO document LIGO-G1501223-v3, <https://dcc.ligo.org/LIGO-G1501223/public>
- Kroupa P., 2001, *MNRAS*, 322, 231
- Loeb A., 2016, *ApJL*, 819, L21
- Luck R. E., Moffett T. J., Barnes III T. G., Gieren W. P., 1998, *AJ*, 115, 605
- Madau P., Dickinson M., 2014, *ARA&A*, 52, 415
- Mapelli M., Zampieri L., Ripamonti E., Bressan A., 2013, *MNRAS*, 429, 2298
- O’Leary R. M., Rasio F. A., Fregeau J. M., Ivanova N., O’Shaughnessy R., 2006, *ApJ*, 637, 937
- Park D., Kim C., Lee H. M., Bae Y.-B., Belczynski K., 2017, *MNRAS*, 469, 4665
- Pelupessy F. I., van Elteren A., de Vries N., McMillan S. L. W., Drost N., Portegies Zwart S. F., 2013, *A&A*, 557, A84
- Pfahl E., Rappaport S., Podsiadlowski P., 2002, *ApJ*, 573, 283
- Planck Collaboration, Ade P. A. R., Aghanim N., Arnaud M., Ashdown M., Aumont J., Baccigalupi C., Banday A. J., Barreiro R. B., Bartlett J. G., et al., 2015, *ArXiv e-prints*
- Portegies Zwart S., McMillan S., Harfst S., Groen D., Fujii M., Nualláin B. Ó., Glebbeek E., Heggie D., Lombardi J., Hut P., Angelou V., Banerjee S., Belkus H., Fragos T., Fregeau J., Gaburov E., Izzard R., Jurić M., Justham S., Sottoriva A., Teuben P., van Bever J., Yaron O., Zemp M., 2009, *New A*, 14, 369
- Portegies Zwart S. F., McMillan S. L. W., 2000, *ApJL*, 528, L17
- Portegies Zwart S. F., McMillan S. L. W., Gieles M., 2010, *ARA&A*, 48, 431
- Portegies Zwart S. F., McMillan S. L. W., Makino J., 2007, *MNRAS*, 374, 95
- Rodriguez C. L., Chatterjee S., Rasio F. A., 2016, *ArXiv e-prints*
- Rodriguez C. L., Morscher M., Pattabiraman B., Chatterjee S., Haster C.-J., Rasio F. A., 2015, *Physical Review Letters*, 115, 051101
- Sheth K., Regan M., Hinz J. L., Gil de Paz A., Menéndez-Delmestre K., Muñoz-Mateos J.-C., Seibert M., Kim T., Laurikainen E., Salo H., Gadotti D. A., Laine J., Mizusawa T., Armus L., Athanassoula E., Bosma A., Buta R. J., Capak P., Jarrett T. H., Elmegreen D. M., Elmegreen B. G., Knapen J. H., Koda J., Helou G., Ho L. C., Madore B. F., Masters K. L., Mobasher B., Ogle P., Peng C. Y., Schinnerer E., Surace J. A., Zaritsky D., Comerón S., de Swardt B., Meidt S. E., Kasliwal M., Aravena M., 2010, *PASP*, 122, 1397
- Spitzer L., 1987, *Dynamical evolution of globular clusters*
- Tanikawa A., 2013, *MNRAS*, 435, 1358
- The LIGO Scientific Collaboration, the Virgo Collaboration, Abbott B. P., Abbott R., Abbott T. D., Abernathy M. R., Acernese F., Ackley K., Adams C., Adams T., et al., 2016, *ArXiv e-prints*
- Vesperini E., 2000, *MNRAS*, 318, 841
- Vink J. S., 2008, *New A Rev.*, 52, 419
- Zaritsky D., Aravena M., Athanassoula E., Bosma A., Comerón S., Elmegreen B. G., Erroz-Ferrer S., Gadotti D. A., Hinz J. L., Ho L. C., Holwerda B., Knapen J. H., Laine J., Laurikainen E., Muñoz-Mateos J. C., Salo H., Sheth K., 2015, *ApJ*, 799, 159
- Zaritsky D., McCabe K., Aravena M., Athanassoula E., Bosma A., Comerón S., Courtois H. M., Elmegreen B. G., Elmegreen D. M., Erroz-Ferrer S., Gadotti D. A., Hinz J. L., Ho L. C., Holwerda B., Kim T., Knapen J. H., Laine J., Laurikainen E., Muñoz-Mateos J. C., Salo H., Sheth K., 2016, *ApJ*, 818, 99
- Zepf S. E., Ashman K. M., 1993, *MNRAS*, 264, 611

